ISSN 1674-1056
http://cpb.iphy.ac.cn
http://iopscience.iop.org/cpb
中国物理 B
Chinese Physics
中国物理 Chinese Physics B

Distributed analysis of forward stimulated Brillouin scattering for acoustic impedance sensing by extraction of a 2nd-order local spectrum

Yu-Lian Yang(杨玉莲), Jia-Bing Lin(林佳兵), Li-Ming Liu(刘黎明), Xin-Hong Jia(贾新鸿), Wen-Yan Liang(梁文燕), Shi-Rong Xu(许世蓉), and Li Jiang(姜利)

Citation: Chin. Phys. B, 2021, 30 (**8**): 084205. DOI: 10.1088/1674-1056/abfcce
Journal homepage: http://cpb.iphy.ac.cn; http://iopscience.iop.org/cpb

What follows is a list of articles you may be interested in

A low-threshold multiwavelength Brillouin fiber laser with double-frequency spacing based on a small-core fiber

Lu-Lu Xu(徐路路), Ying-Ying Wang(王莹莹), Li Jiang(江丽), Pei-Long Yang(杨佩龙), Lei Zhang(张磊), and Shi-Xun Dai(戴世勋)
Chin. Phys. B, 2021, 30 (**8**): 084210. DOI: 10.1088/1674-1056/abff47

Generation of diffraction-free vectorial elliptic hollow beams with space-varying inhomogeneous polarizations

Hui-Rong Li(李会容), Peng-Yi Zhao(赵朋义), and Jian-Ping Yin(印建平)
Chin. Phys. B, 2021, 30 (**8**): 084204. DOI: 10.1088/1674-1056/abe3e9

Generation of wideband tunable femtosecond laser based on nonlinear propagation of power-scaled mode-locked femtosecond laser pulses in photonic crystal fiber

Zhiguo Lv(吕志国) and Hao Teng(滕浩)
Chin. Phys. B, 2021, 30 (**4**): 044209. DOI: 10.1088/1674-1056/abe231

Random-injection-based two-channel chaos with enhanced bandwidth and suppressed time-delay signature by mutually coupled lasers: Proposal and numerical analysis

Shi-Rong Xu(许世蓉), Xin-Hong Jia (贾新鸿), Hui-Liang Ma(马辉亮), Jia-Bing Lin(林佳兵), Wen-Yan Liang(梁文燕), and Yu-Lian Yang(杨玉莲)
Chin. Phys. B, 2021, 30 (**1**): 014203. DOI: 10.1088/1674-1056/abb228

Two-dimensionally controllable DSR generation from dumbbell-shaped mode-locked all-fiber laser

Zhi-Yuan Dou(窦志远), Bin Zhang(张斌), Jun-Hao Cai(蔡君豪), Jing Hou(侯静)
Chin. Phys. B, 2020, 29 (**9**): 094201. DOI: 10.1088/1674-1056/ab9de1

Distributed analysis of forward stimulated Brillouin scattering for acoustic impedance sensing by extraction of a 2nd-order local spectrum*

Yu-Lian Yang(杨玉莲), Jia-Bing Lin(林佳兵), Li-Ming Liu(刘黎明), Xin-Hong Jia(贾新鸿)†, Wen-Yan Liang(梁文燕), Shi-Rong Xu(许世蓉), and Li Jiang(姜利)

College of Physics and Electronic Engineering, Sichuan Normal University, Chengdu 610101, *China*

(Received 8 March 2021; revised manuscript received 22 April 2021; accepted manuscript online 29 April 2021)

Distributed fiber sensors based on forward stimulated Brillouin scattering (F-SBS) have attracted special attention because of their capability to detect the acoustic impedance of liquid material outside fiber. However, the reported results were based on the extraction of a 1st-order local spectrum, causing the sensing distance to be restricted by pump depletion. Here, a novel post-processing technique was proposed for distributed acoustic impedance sensing by extracting the 2nd-order local spectrum, which is beneficial for improving the sensing signal-to-noise ratio (SNR) significantly, since its pulse energy penetrates into the fiber more deeply. As a proof-of-concept, distributed acoustic impedance sensing along ∼ 1630 m fiber under moderate spatial resolution of ∼ 20 m was demonstrated.

Keywords: distributed acoustic impedance sensing, forward stimulated Brillouin scattering (F-SBS), 2nd-order local spectrum

PACS: 42.81.−i, 42.81.Pa, 78.35.+c **DOI:** 10.1088/1674-1056/abfcce

1. Introduction

Stimulated Brillouin scattering (SBS) is a nonlinear interaction due to electrostriction and elastic-optics effects between acoustic, pump and Stokes waves, which can be categorized into backward and forward scattering (B-SBS[1–4]/F-SBS). B-SBS is caused by longitudinal acoustic waves in fiber. In this case, the acoustic wave is bound inside the core and incapable of interacting with the outside surroundings directly. When only pump light is injected into a fiber, transverse acoustic modes can be stimulated. This spontaneous scattering is called guided acoustic wave Brillouin scattering (GAWBS).[5–8] The types of transverse acoustic wave in GAWBS include radial (R_{0m}) and torsional–radial modes (TR_{2m}).[5] At present, the characteristics of GAWBS of many different types of optical fibers have been reported.[6–24] When both pump and Stokes lights are injected in the same direction, and if their frequency difference is equal to the resonance frequency of R_{0m} or TR_{2m} modes, F-SBS can be activated.

Because the transverse acoustic resonance can penetrate into the cladding of fiber and sense the mechanical properties of material outside the fiber, GAWBS and F-SBS have recently been proposed to detect the acoustic impedance (defined as the product of acoustic velocity and density) of liquid materials outside optical fibers,[25–35] which can be regarded as a new class of fiber sensors. In addition, this striking effect has been extensively used for acoustic velocity measurement,[36] fiber diameter estimation,[37] temperature and strain sensing,[38–41] and pulse amplification for Brillouin optical time-domain analysis (BOTDA).[42] The sensing applications of acoustic impedance include point-type[25–29] and distributed measurements.[30–35] Compared with point-type sensors, a key advantage of distributed sensors lies in the multi-point simultaneous measurement. The group of Zadok demonstrated distributed acoustic-impedance sensing along ∼ 3 km optical fiber with 100 m spatial resolution by demodulating Rayleigh scattering of pump and Stokes pulses, also known as opto-mechanical time-domain reflectometry (OMTDR).[30] The group of Thévenaz utilized long pump–Stoke pulses to excite a transverse acoustic field, followed by a short reading pulse to detect the induced cross-phase modulation (XPM). Based on this approach, 730 m sensing with 15 m spatial resolution has been achieved.[32] The spatial resolution can be further improved to 8 m (along ∼ 650 m fiber) by probing with Brillouin optical time-domain reflectometry (BOTDR).[33] Moreover, Dong's group proposed a novel opto-mechanical time-domain analysis (OMTDA) based on coherent F-SBS probing to enhance the signal-to-noise ratio (SNR), and acoustic impedance sensing with high spatial resolution up to 2 m along 225 m fiber was obtained.[34]

Nevertheless, the reported performances of distributed F-SBS sensing are far worse than those of B-SBS-based sensors, such as BOTDA and BOTDR. This is attributed to two reasons.

*Project supported by the Sichuan Science and Technology Program (Grant No. 2019YJ0530), Scientific Research Fund of Sichuan Provincial Education Department, China (Grant No. 18ZA0401), and the National Natural Science Foundation of China (Grant No. 61205079).

†Corresponding author. E-mail: jiaxh_0@126.com

© 2021 Chinese Physical Society and IOP Publishing Ltd

Firstly, the relatively weak gain coefficient [$\sim 5\ \mathrm{W}^{-1}\cdot\mathrm{km}^{-1}$ for standard single-mode fiber (SMF)[24,30]] of F-SBS restricts the sensing SNR and makes further distance extension very challenging due to nonlinear effects caused by high pulse peak powers (Watt level). Secondly, the reported results were based on the extraction of a 1st-order local spectrum,[30–35] which is only concentrated on the front end of a fiber, due to the intensified pump depletion from a higher-order sideband towards the far end. These factors restrict the sensing distance within 1 km typically for moderate and high spatial resolution.[32–35] Note that beyond 1 km sensing distance was also possible; however, this was achieved at the expense of relatively lower spatial resolution (100 m).[30,31]

In this work, a novel post-processing method for distributed acoustic impedance sensing based on the extraction of the 2nd-order local spectrum was proposed. In our scheme, sensing of the SNR and distance can be effectively improved by extracting the cascaded 2nd- and 1st-order local spectrums of F-SBS.

2. Operation principle and experimental setup

Figure 1 shows a schematic diagram of the proposed distributed F-SBS sensors using one of the 2nd-order sidebands for local spectrum extraction. The dual-sidebands' optical pulses with enough long duration are used to activate F-SBS. The duration should be far larger than the phonon lifetime in the F-SBS process.[30–35] Note that in contrast to Ref. [32], the key point of the proposed method lies in the post-processing procedure for the acquired 1st- and 2nd-order sidebands, in order to extract the 2nd-order local spectrum for sensing distance extension, instead of extracting only the 1st-order local spectrum.[32] The frequency separation of ~ 322 MHz denoted by $2\Delta\nu$ corresponds to the transverse acoustic resonance of the strongest R_{07} mode.[30–35] A reading pulse is then followed to detect the induced XPM by F-SBS. Due to the frequency shift ($\nu_{\mathrm{AOM}} = 200$ MHz) of the used acoustic-optic modulator (AOM), frequency separation between the probe light and optical source of the reading pulse (represented by dotted lines) should be centered around $\nu_{\mathrm{B}} + \nu_{\mathrm{AOM}} + 2\Delta\nu$ [see Fig. 1(a)] and $\nu_{\mathrm{B}} + \nu_{\mathrm{AOM}} + 4\Delta\nu$ [see Fig. 1(b)], respectively, where ν_{B} (~ 10790 MHz) is the Brillouin frequency shift (BFS) of the fiber under test (FUT). With the increase in pump–Stokes powers, depletion of 1st-order sidebands is strengthened, whereas $\pm$ 2nd-order sidebands are gradually excited. Using BOTDA technology, power evolutions of the scattered 1st- and 2nd-order pulses can be obtained. To suppress the impact of position-dependent BFS variation, scanning of the sidebands is implemented within ± 30 MHz in 3 MHz steps for each $2\Delta\nu$. Therefore, we can obtain the traces of sidebands by summing the Brillouin gain spectrum (BGS) of BOTDA.[34]

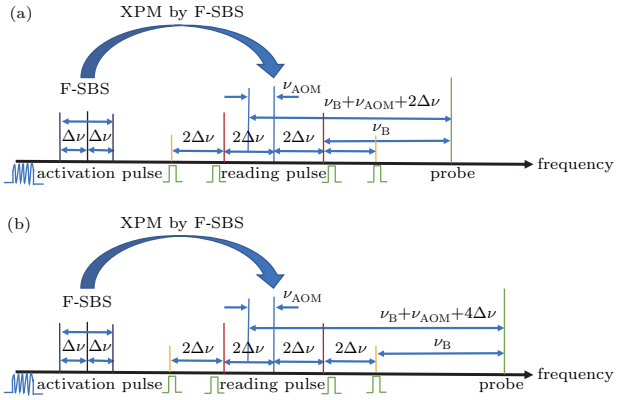


Fig. 1. A principle diagram of distributed F-SBS sensors based on proposed 2nd-order local spectrum extraction. In the post-processing stage, the combined 2nd- and 1st-order local spectrums are used to extend the sensing distance. The dotted lines are the positions of the optical source for the reading pulse.

Considering the influence of acoustic impedance of external material in fiber, the F-SBS resonance linewidth $\Delta\upsilon_m$ is given by[28,29,32–34]

$$\Delta\upsilon_{\mathrm{m}} = \Delta\upsilon_{\mathrm{int}} + (\Delta\upsilon_{\mathrm{i}}/\pi)\ln(1/|r_{\mathrm{mir}}|), \tag{1}$$

where $\Delta\upsilon_{\mathrm{m}}$ is the measured F-SBS linewidth, and $\Delta\upsilon_{\mathrm{int}}$ and $\Delta\upsilon_{\mathrm{i}}$ are the intrinsic F-SBS linewidth and frequency separation (~ 48 MHz) between two adjacent F-SBS spectral resonances. The reflectivity coefficient r_{mir} of the phonon at the boundary of cladding and outside material is defined as[28,29,32–34]

$$|r_{\mathrm{mir}}| = |Z_{\mathrm{f}} - Z_{\mathrm{o}}| / (Z_{\mathrm{f}} + Z_{\mathrm{o}}), \tag{2}$$

where Z_{f} ($Z_{\mathrm{f}} = 13.1 \times 10^6\ \mathrm{kg/m^2\cdot s}$[32]) and Z_{o} are acoustic impedances of silica and external material, respectively.

The local refractive index variation induced by F-SBS is proportional to $\mathrm{d}[2(I_1/I_0)^{1/2}]/\mathrm{d}z$ for the reported 1st-order spectrum[32,33] or $\mathrm{d}[4(I_2/I_1)^{1/2}]/\mathrm{d}z$ for the proposed post-processing based on the 2nd-order spectrum approximately, where I_0, I_1, and I_2 are the powers of 0th-, 1st-, and 2nd-order sidebands. The detailed principle of the used post-processing method is explained briefly.

Considering the F-SBS induced XPM, the optical field of the reading pulse $E(\upsilon_{\mathrm{F}}, z_{\mathrm{r}}, t)$ can be written as[32]

$$\begin{aligned} E(\upsilon_{\mathrm{F}}, z_{\mathrm{r}}, t) &= A(z_{\mathrm{r}}, t)\exp[j(k_z z_{\mathrm{r}} - \omega_0 t + \varphi_0)] \\ &\quad \times \exp[j\xi(\upsilon_{\mathrm{F}}, z_{\mathrm{r}})\cos(2\pi\upsilon_{\mathrm{F}} t)], \end{aligned} \tag{3}$$

where $\upsilon_{\mathrm{F}} = 2\Delta\nu$ is frequency detuning, t is the time, z_{r}, ω_0, $k_z = 2\pi/\lambda$ are the spatial position, angular frequency and wave-vector of the reading pulse, respectively, $A(z_{\mathrm{r}}, t)$ is the slowly variable amplitude of the reading pulse, and φ_0 is the initial phase. The phase factor $\xi(\upsilon_{\mathrm{F}}, z_{\mathrm{r}})$ due to F-SBS can be described as[32]

$$\xi(\upsilon_{\mathrm{F}}, z_{\mathrm{r}}) = \frac{2\pi}{\lambda}\int_0^{z_{\mathrm{r}}} a_{\mathrm{RI}}(\upsilon_{\mathrm{F}}, z)\,\mathrm{d}z, \tag{4}$$

where $a_{\mathrm{RI}}(\upsilon_{\mathrm{F}}, z_{\mathrm{r}})$ is the induced refractive index distribution due to F-SBS. Using Bessel expansion, Eqs. (3) and (4) can be rewritten as[32]

$$E(\upsilon_{\mathrm{F}},z_{\mathrm{r}},t) = A(z_{\mathrm{r}},t)\exp[j(k_z z_{\mathrm{r}}+\varphi_0)]\sum_{n=-\infty}^{\infty}\{j^n J_n[\xi(\upsilon_{\mathrm{F}},z_{\mathrm{r}})] \times \exp[-j(\omega_0-2\pi\upsilon_{\mathrm{F}}n)t]\}, \quad (5)$$

where $J_n(\xi)$ is the nth-order Bessel function of ξ. Equation (5) clearly shows the generation of multiple sidebands caused by F-SBS. The intensity of each sideband is given by $I_n = A^2(z_{\mathrm{r}},t)J_n^2$. The relationship of the adjacent sidebands is given by[43]

$$J_{n-1}[\xi(\upsilon_{\mathrm{F}},z_{\mathrm{r}})]+J_{n+1}[\xi(\upsilon_{\mathrm{F}},z_{\mathrm{r}})] = \frac{2n}{\xi(\upsilon_{\mathrm{F}},z_{\mathrm{r}})}J_n[\xi(\upsilon_{\mathrm{F}},z_{\mathrm{r}})]. \quad (6)$$

For a typical $\xi(\upsilon_{\mathrm{F}}, z_{\mathrm{r}})$ range [for example, within $0 \le \xi(\upsilon_{\mathrm{F}},z_{\mathrm{r}}) \le 2.4048$], the values of $J_n[\xi(\upsilon_{\mathrm{F}},z_{\mathrm{r}})]$ $(n = 0,1,2,3)$ are positive. Considering that generally $I_0 \gg I_2$ and $I_1 \gg I_3$, let $n = 1$ (conventional method), we have[32]

$$\xi(\upsilon_{\mathrm{F}},z_{\mathrm{r}}) \approx 2\frac{J_1[\xi(\upsilon_{\mathrm{F}},z_{\mathrm{r}})]}{J_0[\xi(\upsilon_{\mathrm{F}},z_{\mathrm{r}})]} = 2\frac{I_1^{1/2}[\xi(\upsilon_{\mathrm{F}},z_{\mathrm{r}})]}{I_0^{1/2}[\xi(\upsilon_{\mathrm{F}},z_{\mathrm{r}})]}. \quad (7a)$$

For $n = 2$ (the method used in this work), a similar expression can be derived as

$$\xi(\upsilon_{\mathrm{F}},z_{\mathrm{r}}) \approx 4\frac{J_2[\xi(\upsilon_{\mathrm{F}},z_{\mathrm{r}})]}{J_1[\xi(\upsilon_{\mathrm{F}},z_{\mathrm{r}})]} = 4\frac{I_2^{1/2}[\xi(\upsilon_{\mathrm{F}},z_{\mathrm{r}})]}{I_1^{1/2}[\xi(\upsilon_{\mathrm{F}},z_{\mathrm{r}})]}. \quad (7b)$$

The refractive index change induced by XPM of F-SBS can be obtained by derivation of $\xi(\upsilon_{\mathrm{F}}, z_{\mathrm{r}})$ along z from Eq. (4).

The experimental setup is described in Fig. 2. The basic structure is similar to that in Ref. [32], except for the post-processing procedure used to extract the 2nd-order local spectrum. The activation and reading branches are generated by two distributed-feedback laser-diodes (DFB-LDs). For the activation branch, output from DFB-LD2 at 1550.7 nm is used to produce dual-sideband activation lights with a carrier-suppressed electro-optic modulator (EOM2). Frequency scanning around 322 MHz is performed by varying the frequency of the micro-wave source (MWS2) to obtain the F-SBS gain spectrum.[30–35] AOM2, driven by an arbitrary waveform generator (AWG), is utilized to generate pump and Stokes pulses of $\sim$ 400 ns duration.

With regard to the reading branch, emission from DFB-LD1 at $\sim$ 1549.3 nm is split into two paths. The upper one is used to generate the probing continuous wave (CW) by a carrier-suppressed EOM1, which is driven by MSW1. As has been mentioned, the driving frequency of the probe should correspond to 1st- and 2nd-order sidebands. Note that another DFB-LD3 is injection-locked by the weak high-frequency sideband. This new design can avoid the excessive noise if optical amplification is introduced in this branch. Also, the instability during frequency scanning of MSW1 (due to frequency-dependent power variation) can be overcome radically. The reading pulse with $\sim$ 150 ns width is formed using AOM1, corresponding to $\sim$ 15 m spatial resolution in theory. To suppress the polarization-dependent noise, two polarization scramblers are introduced for both the probe CW and the 0th-order reading pulse. Three erbium-doped fiber amplifiers (EDFAs) are employed to boost the peak powers of the activation and reading pulses.

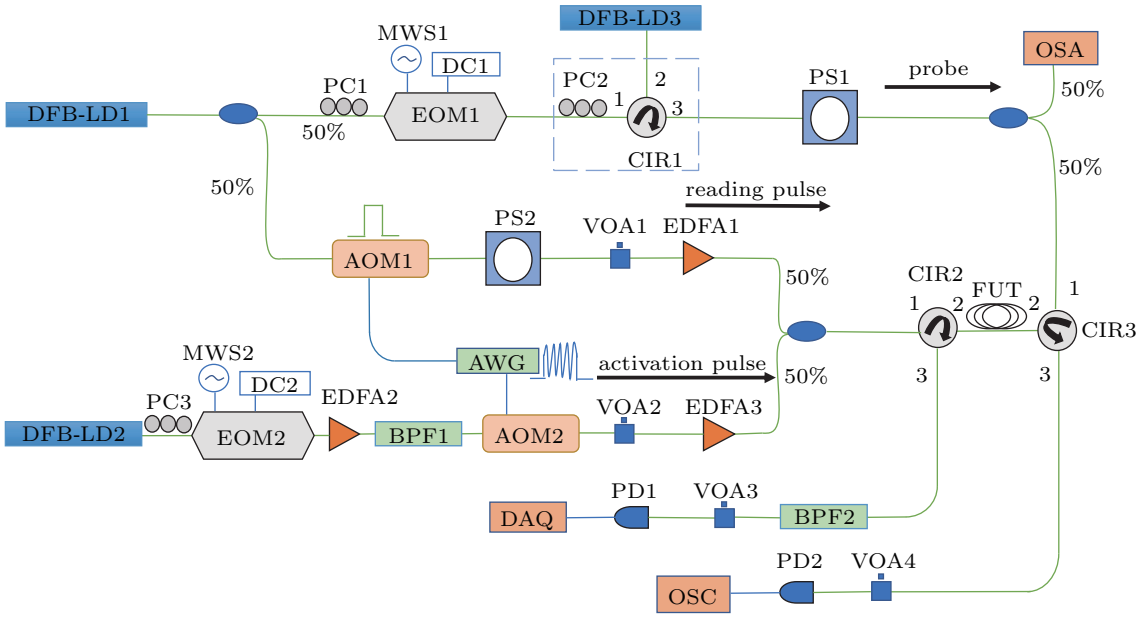


Fig. 2. The experimental setup of distributed F-SBS sensors based on 2nd-order local spectrum extraction. DFB-LD: distributed feedback laser diode; EOM: electro-optic modulator; MWS: micro-wave source; DC: direct current; PS: polarization scrambler; PC: polarization controller; AOM: acousto-optic modulator; AWG: arbitrary waveform generator; CIR: circulator; EDFA: erbium-doped fiber amplifier; BPF: bandpass filter; VOA: variable optical attenuator; FUT: fiber under test; PD: photodetector; OSA: optical spectrum analyzer; OSC: oscilloscope; DAQ: data acquisition card.

At the receiver end, a narrower (< 0.1 nm) band pass filter (BPF2) is applied to eliminate the Rayleigh scattering and facet-end reflection of activation and reading pulses. The sampling rate of the data acquisition card (DAQ) is 100 MSa/s.

3. Experimental results and discussion

In the experiment, SMF is used as the FUT. The F-SBS gain spectrum is characterized by scanning the pump–Stokes detuning (314–330 MHz) with an increment of 0.2 MHz. The power of the probe CW injected into the FUT is ~ -1 dBm. The used peak powers of the activation and reading pulses are ~ 37.3 dBm (per sideband) and 33 dBm, respectively. The averaging times for each sweep of MWS1 are 500. As has been mentioned, 21 times frequency scanning of MSW1 is implemented within ± 30 MHz in 3 MHz steps for each frequency of F-SBS, so the total scanning time is $10500 = 500 \times 21$. At the far end, the coating layer of a 15 m segment is removed, and then placed in air, ethanol and water, respectively, to measure the acoustic impedance of the surrounding liquids.[30–35]

Figures 3(a) and 3(b) show the 3-D power distributions of 1st- and 2nd-order sidebands, respectively. In the air-exposed region, two particularly steep slopes occur due to the higher acoustic reflectivity at the boundary between cladding and air. As seen from Fig. 3(a), the 1st-order gain spectrum starts to be saturated considerably after ~ 780 m by the depletion from the 2nd-order spectrum. Note that although the saturation can be weakened by decreasing the pump and Stokes powers, the slope and sensing distance will be sacrificed significantly. Another feature is that, compared with the 2nd-order sideband, spectral broadening is experienced for the 1st-order sideband towards the far end of the fiber (~ 7 MHz maximum).

The observed power distributions for both the 0th-order (not shown here) and 1st-order sidebands [$>\sim 780$ m, see Fig. 3(a)] exhibit large polarization noises, seriously restricting the sensing SNR. Here, to alleviate this impact, we normalize the measured sidebands with a trace when a reading pulse with lower peak power (~ 14 dBm) is injected without F-SBS, so that the additional loss and polarization noise can be perfectly compensated. Note that before the derivation operation, a moving average is used to further suppress the noise,[30–35] leading to a real spatial resolution of ~ 20 m.

Figure 3(c) shows the retrieved 2nd-order local spectrum distribution of F-SBS along the whole FUT, where the uncoated segment exposed in air can be identified clearly. The details of other subsections, except for the uncoated segment, are shown in Fig. 3(d). It is observed that the 2nd-order local spectrum shows a higher SNR after ~ 780 m. Since the local spectrum results from the convolution of the rectangular-shaped pulse spectrum (sinc function) and original F-SBS spectrum (Lorentzian function), the spectrum width of the air-exposed segment is almost dominated by the pulse spectrum.[32] As a comparison, Fig. 3(e) plots the retrieved 1st-order local spectrum of F-SBS in the range of 0–1.2 km based on the conventional method.[32] The SNR becomes very poor after ~ 780 m due to pump depletion from the 2nd-order sideband. Thus, sensing information along the whole FUT can be extracted using a combination of 1st- and proposed 2nd-order local spectrums for the ranges of [0 780] m and [780 1630] m, respectively.

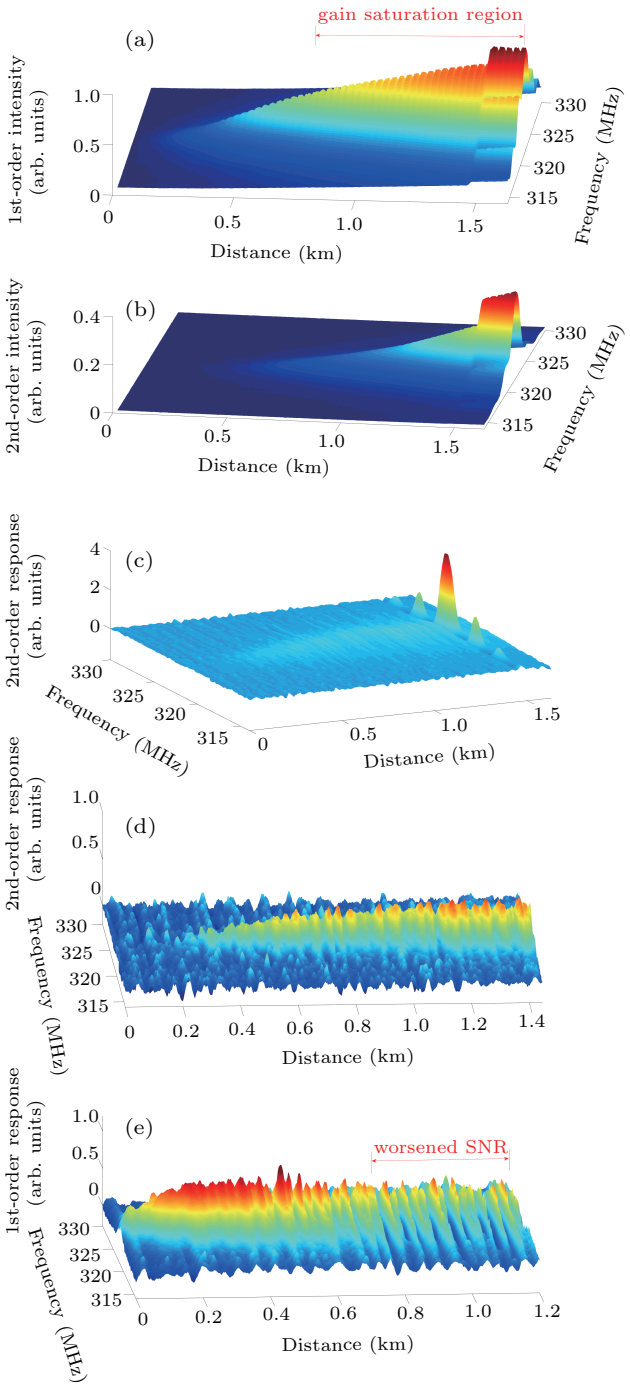


Fig. 3. (a) The 3-D power distributions of the 1st-order sideband; (b) 3-D power distributions of the 2nd-order sideband; (c) the retrieved 2nd-order local spectrum of F-SBS along the whole FUT using the proposed post-processing method; (d) the detail of (c), except for the uncoated segment; (e) the retrieved 1st-order local spectrum of F-SBS in the range of $0 \sim 1.2$ km.

Figure 4(a) depicts the retrieved 2nd-order local spectrum of the sensing point in different outside liquids. The observed FWHM of the coated segment is ~ 5.6 MHz, while it becomes ~ 1.8 MHz, 3.5 MHz, and 4.8 MHz, respectively, when the uncoated segment is exposed in air, absolute ethanol and water. In order to remove the impact of the pulse spectrum and obtain the intrinsic spectrum width, a convolution formula[44] is used to fit the local F-SBS spectrum $g_T(\Omega)$,[32,33] written as

$$g_T(\Omega) = g_B(\Omega)\left\{1 - \frac{(\Gamma^2 - \Omega^2)\left[1 - e^{-\Gamma T}\cos(T\Omega)\right] + 2\Gamma\Omega e^{-\Gamma T}\sin(T\Omega)}{\Gamma T(\Gamma^2 + \Omega^2)}\right\}, \tag{8}$$

where $g_B(\Omega)$ is the F-SBS gain with Lorentz shape, T is the duration of the used pulse, $\Omega = 2\pi f$ is the angular frequency detuning, and $\Gamma = \pi\Delta\upsilon_m$ is the half-width at half maximum (HWHM) of $g_B(\Omega)$.

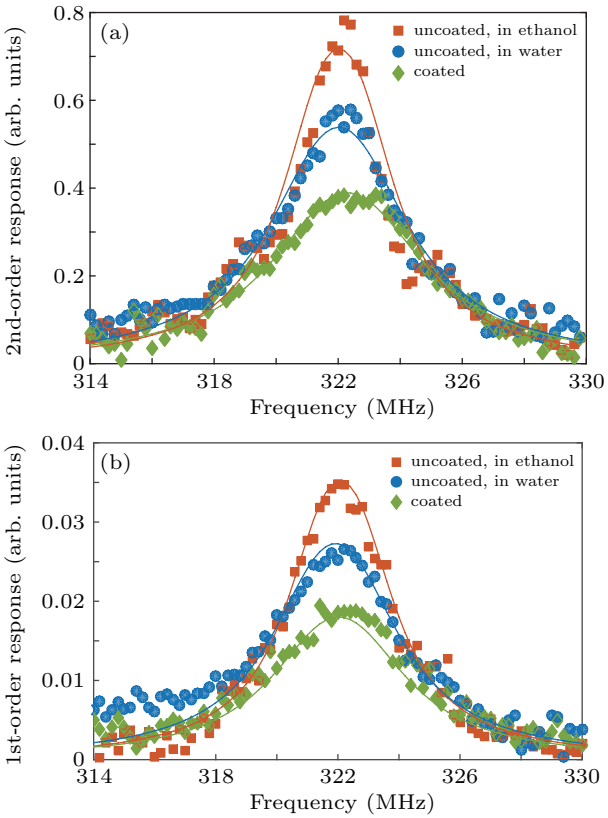


Fig. 4. Retrieved 2nd-order (a) and 1st-order (b) local spectrums of the sensing point in different outer liquids. The solid lines are fitted curves using the spectral convolution formula from Eq. (8). In (a) and (b), the ~ 15 m unjacketed segment is located at the far end and front end ($z \sim 630$ m), respectively.

The extracted linewidths are ~ 0.3 MHz, 2.7 MHz, and 4.2 MHz when immersed in air, absolute ethanol and water. Using Eqs. (1) and (2), the measured acoustic impedances of the surrounding materials are ~ 1.01×10^6 kg/m^2·s and 1.67×10^6 kg/m^2·s for ethanol and water, respectively. These results agree well with the standard values (0.93×10^6 kg/m^2·s and 1.483×10^6 kg/m^2·s for ethanol and water).[32] We also extract the linewidths of F-SBS when the ~ 15 m segment is unjacketed and immersed into liquids at the front end ($z \sim 630$ m) using the conventional 1st-order local spectrum, as shown in Fig. 4(b). The extracted linewidths are ~ 0.4 MHz, 2.7 MHz, and 3.9 MHz when immersed in air, ethanol, and water, respectively, and the corresponding acoustic impedances are ~ 1.0×10^6 kg/m^2·s and 1.48×10^6 kg/m^2·s for ethanol and water, respectively. These results are close to that using the 2nd-order local spectrum. Note that the acoustic impedance for the section of [780 1630] m is difficult to retrieve correctly using the conventional 1st-order local spectrum, as shown in Fig. 3(e).

4. Conclusion

In summary, in order to solve the SNR degradation due to power depletion for reported F-SBS sensors using the 1st-order local spectrum of F-SBS, a novel post-processing method was proposed and demonstrated by extracting the 2nd-order local spectrum to extend the sensing distance. This measurement is complementary to the 1st-order case, as its pulse energy is concentrated mainly towards the far end of the FUT. As a proof-of-concept, ~ 1630 m sensing distance under moderate spatial resolution of ~ 20 m was demonstrated. In order to further extend the sensing distance and improve the spatial resolution, the proposed approach could also be generalized to 3rd- or higher-order spectrum measurements. Although the required pump–Stokes peak power in this work is higher than the 1st-order case[32] by ~ 2.3 dB, combining it with high nonlinear fiber (HNLF)[24] or dispersion compensation fiber (DCF) can easily overcome this shortcoming, due to the lower effective area of these fibers.

References

[1] Wang S H, Ren L Y and Liu Y 2009 *Acta Phys. Sin.* **58** 3943 (in Chinese)
[2] Zhang Y C, Chen W, Sun S L and Meng Z 2015 *Chin. Phys. B* **24** 094209
[3] Mu K L, Shang J M, Tang L H, Wang Z K, Yu S and Qiao Y J 2019 *Chin. Phys. B* **28** 094216
[4] Wang G, Xu L X and Gu C 2018 *Chin. Phys. Lett.* **35** 084201
[5] Shelby R M, Levenson M D and Bayer P W 1985 *Phys. Rev. B.* **31** 5244
[6] Townsend P D, Poustie A J, Hardman P J and Blow K J 1996 *Opt. Lett.* **21** 333
[7] Biryukov A S, Sukharev M E and Dianov E M 2002 *Quantum Electron.* **32** 765
[8] Quang D L, Jaouën Y, Zimmerli M, Gallion P and Thomine J B 1996 *IEEE Photon. Technol. Lett.* **8** 414
[9] Russell P St J, Culverhouse D and Farahi F 1990 *Electron. Lett.* **26** 1195

[10] Russell P St J, Culverhouse D and Farahi F 1991 *IEEE J. Quantum Electron.* **27** 836
[11] Matsui T, Nakajima K and Yamamoto F 2015 *Appl. Opt.* **54** 6093
[12] Nishizawa N, Kume S, Mori M and Goto T 1995 *J. Opt. Soc. Am. B.* **12** 1651
[13] Kang M S, Brenn A, Wiederhecker G S and Russell P St J 2008 *Appl. Phys. Lett.* **93** 131110
[14] Koehler J R, Butsch A, Euser T G, Noskov R E and Russell P St J 2013 *Appl. Phys. Lett.* **103** 221107
[15] Butsch A, Koehler J R, Noskov R E and Russell P St J 2014 *Optica* **1** 158
[16] Koehler J R, Noskov R E, Sukhorukov A A, Butsch A, Novoa D and Russell P St J 2016 *APL Photonics* **1** 056101
[17] Wiederhecker G S, Brenn A, Fragnito H L and Russell P St J 2008 *Phys. Rev. Lett.* **100** 203903
[18] Dainese P, Russell P St J, Joly N, Knight J C, Wiederhecker G S, Fragnito H L, Laude V and Khelif A 2006 *Nat. Phys.* **2** 388
[19] Dainese P, Russell P St J, Wiederhecker G S, Joly N, Fragnito H L, Laude V and Khelif A 2006 *Opt. Express.* **14** 4141
[20] Brenn A, Wiederhecker G S, Kang M S, Hundertmark H, Joly N and Russell P St J 2009 *J. Opt. Soc. Am. B.* **26** 1641
[21] Beugnot J C and Laude V 2012 *Phys. Rev. B.* **86** 224304
[22] Diamandi H H, London Y and Zadok A 2017 *Optica* **4** 289
[23] Diamandi H H, London Y, Bashan G, Bergman A and Zadok A 2018 *Sci. Rep.* **8** 9514
[24] London Y, Diamandi H H and Zadok A 2017 *APL Photonics.* **2** 041303
[25] Antman Y, Clain A, London Y and Zadok A 2016 *Optica* **3** 510
[26] Chow D M, Soto M A and Thévenaz L 2017 *25th International Conference on Optical Fibre Sensors* **10323** 1032311
[27] Hayashi N, Mizuno Y, Nakamura K, Set S Y and Yamashita S 2017 *Opt. Express.* **25** 2239
[28] Chow D M and Thévenaz L 2018 *Opt. Lett.* **43** 5467
[29] Zheng Z, Li Z, Fu X, Wang L and Wang H 2020 *Opt. Lett.* **45** 4523
[30] Bashan G, Diamandi H H, London Y, Preter E and Zadok A 2018 *Nat. Commun.* **9** 2991
[31] Diamandi H H, London Y, Bashan G and Zadok A 2019 *APL Photonics* **4** 016105
[32] Chow D M, Yang Z, Soto M A and Thévenaz L 2018 *Nat. Commun.* **9** 2990
[33] Zaslawski S, Yang Z, Wang S and Thévenaz L 2019 *Seventh European Workshop on Optical Fibre Sensors* **11199** 1119923
[34] Pang C, Hua Z, Zhou D, Zhang H, Chen L, Bao X Y and Dong Y K 2020 *Optica* **7** 176
[35] Zaslawski S, Yang Z and Thévenaz L 2021 *Optica* **8** 388
[36] Shiraki K and Ohashi M 1992 *IEEE Photon. Technol. Lett.* **4** 1177
[37] Ohashi M, Shibata N and Shiraki K 1992 *Electron. Lett.* **28** 900
[38] Tanaka Y and Ogusu K 1998 *IEEE Photon. Technol. Lett.* **10** 1769
[39] Carry E, Beugnot J C, Stiller B, Lee M W, Maillotte H and Sylvestre T 2011 *Appl. Opt.* **50** 6543
[40] Hayashi N, Suzuki K, Set S Y and Yamashita S 2017 *Appl. Phys. Express.* **10** 092501
[41] Tanaka Y and Ogusu K 1999 *IEEE Photon. Technol. Lett.* **11** 865
[42] Lin J B, Jia X H, Xu S R, Ma H L, Wu H and Wei X Y 2019 *Appl. Phys. Express.* **12** 102014
[43] Goldstein M and Thaler R M 1959 *Math. Comput.* **13** 102
[44] Alem M, Soto M A, Tur M and Thévenaz L 2017 *25th Optical Fiber Sensors Conference* 1